



# Radiative Transfer Simulation for the Optical and Near-infrared Electromagnetic Counterparts to GW170817

Kyohei Kawaguchi<sup>1,2,3</sup>, Masaru Shibata<sup>2,3</sup> , and Masaomi Tanaka<sup>4,5</sup> 

<sup>1</sup>Institute for Cosmic Ray Research, The University of Tokyo, 5-1-5 Kashiwanoha, Kashiwa, Chiba 277-8582, Japan

<sup>2</sup>Max Planck Institute for Gravitational Physics (Albert Einstein Institute), Am Mühlenberg 1, Potsdam-Golm, D-14476, Germany

<sup>3</sup>Center for Gravitational Physics, Yukawa Institute for Theoretical Physics, Kyoto University, Kyoto, 606-8502, Japan

<sup>4</sup>Astronomical Institute, Tohoku University, Aoba, Sendai 980-8578, Japan

<sup>5</sup>National Astronomical Observatory of Japan, Mitaka, Tokyo, Japan

Received 2018 April 15; revised 2018 August 13; accepted 2018 August 29; published 2018 September 27

## Abstract

Recent detection of gravitational waves from a binary neutron star merger (GW170817) and the subsequent observations of electromagnetic counterparts provide a great opportunity to study the physics of compact binary mergers. The optical and near-infrared counterparts to GW170817 (SSS17a, also known as AT 2017gfo or DLT17ck) are found to be consistent with a kilonova/macronova scenario with red and blue components. However, in most previous studies wherein the contribution from each ejecta component to the lightcurves is separately calculated and composited, the red component is too massive of a dynamical ejecta, and the blue component is too fast of a post-merger ejecta. In this Letter, we perform a two-dimensional radiative transfer simulation for a kilonova/macronova, consistently taking the interplay of multiple ejecta components into account. We show that the lightcurves and photospheric velocity of SSS17a can be reproduced naturally by a setup that is consistent with the prediction of the numerical-relativity simulations.

*Key words:* gravitational waves – nuclear reactions, nucleosynthesis, abundances – radiative transfer – stars: neutron

## 1. Introduction

On 2017 August 17, the first detection of gravitational waves from a binary neutron star (NS) merger referred to as GW170817 was achieved by three ground-based detectors (Abbott et al. 2017a). Electromagnetic (EM) counterparts to GW170817 were observed over the entire wavelength range. Gamma-ray signals were detected about 1.7 seconds after the onset of the merger (Abbott et al. 2017b). Then a counterpart in ultraviolet, optical, and near-infrared (NIR) wavelengths, named SSS17a (also known as AT 2017gfo or DLT17ck), was discovered (e.g., Coulter et al. 2017; Cowperthwaite et al. 2017; Drout et al. 2017; Kasliwal et al. 2017; Smartt et al. 2017; Tanvir et al. 2017; Valenti et al. 2017, see more references in Villar et al. 2017). NGC 4993, a galaxy at a distance of 40 Mpc, was identified as the host galaxy of GW170817 by the EM signals. X-ray (e.g., Troja et al. 2017) and radio signals (e.g., Mooley et al. 2017) were also detected subsequently.

Among various EM signals from NS mergers, the emission in optical and NIR wavelengths is of particular interest. It has been suggested that a fraction of NS material would be ejected from the system during the merger (e.g., Rosswog et al. 1999; Hotokezaka et al. 2013), and heavy radioactive nuclei would be synthesized in the ejecta by the so-called  $r$ -process nucleosynthesis (Lattimer & Schramm 1974; Eichler et al. 1989; Korobkin et al. 2012; Wanajo et al. 2014). It has been predicted that EM emission in optical and NIR wavelengths could occur through the radioactive decays of heavy elements (Li & Paczynski 1998; Kulkarni 2005; Metzger et al. 2010; Kasen et al. 2013; Tanaka & Hotokezaka 2013). This emission is called a “kilonova” or “macronova.” Previous studies (Li & Paczynski 1998; Kasen et al. 2013, 2015; Barnes et al. 2016; Tanaka et al. 2017, 2018; Wollaeger et al. 2017) have shown that lightcurves of kilonovae/macronovae depend on the mass, velocity, and electron fraction

( $Y_e$ , number of protons per nucleon which controls the final element abundances) of ejecta. These quantities reflect the mass ejection mechanism, and thus, we can study the physical process of an NS merger and associated  $r$ -process nucleosynthesis via detailed analysis of kilonovae/macronovae lightcurves.

Several ejection mechanisms are proposed for NS mergers. One is called dynamical ejection, which is driven by tidal interaction and shock heating during the collision of NSs (Bauswein et al. 2013; Hotokezaka et al. 2013; Radice et al. 2016; Sekiguchi et al. 2016; Bovard et al. 2017; Dietrich et al. 2017). Numerical relativity simulations for binary NS mergers show that the mass and averaged velocity of the dynamical ejecta are typically  $10^{-3}$ – $10^{-2} M_{\odot}$  and  $0.15$ – $0.25 c$ , respectively, where  $c$  is the speed of light. The electron fraction is distributed in the range of  $0.05$ – $0.5$ , which leads to a large value of opacity  $\sim 10 \text{ cm}^2 \text{ g}^{-1}$  (Kasen et al. 2013; Tanaka & Hotokezaka 2013). Due to such high opacity, the kilonova/macronova emission from the dynamical ejecta is expected to be bright in NIR wavelengths and last for  $\sim 10$  days (hereafter referred to as the red component). After the dynamical ejection, the mass ejection from the merger remnant driven by viscous and neutrino heating follows (referred to as post-merger ejecta; Dessart et al. 2009; Metzger & Fernández 2014; Perego et al. 2014; Just et al. 2015; Lippuner et al. 2017; Shibata et al. 2017; Siegel & Metzger 2017; Fujibayashi et al. 2018). Numerical-relativity simulations considering the effects of physical viscosity and neutrino radiation show that  $10^{-2}$ – $10^{-1} M_{\odot}$  of the material can be ejected typically with the velocity of  $\lesssim 0.1 c$  from the massive NS and torus formed after the merger. Due to the irradiation by neutrinos emitted from the remnant NS, the electron fraction of the post-merger ejecta typically has a larger value than that of the dynamical ejecta, and in particular,  $Y_e \approx 0.3$ – $0.4$  could be realized if the remnant NS is sufficiently long-lived ( $\sim 1$  s; Metzger & Fernández 2014; Lippuner et al. 2017; Fujibayashi et al. 2018). This leads to a

smaller value of opacity  $\sim 0.1\text{--}1\text{ cm}^2\text{ g}^{-1}$  (Kasen et al. 2015; Tanaka et al. 2018), and hence, blue optical emission that lasts for  $\sim 1$  day would occur (hereafter referred to as the blue component).

A number of studies have shown that SSS17a is consistent with kilonova/macronova models composed of red and blue (or more) components (e.g., Cowperthwaite et al. 2017; Kasen et al. 2017; Kasliwal et al. 2017; Villar et al. 2017). However, (i) the estimated mass for the red component,  $10^{-2}\text{--}10^{-1} M_{\odot}$ , is more massive than the theoretical prediction for the dynamical ejecta ( $\lesssim 0.01 M_{\odot}$ ; Bauswein et al. 2013; Hotokezaka et al. 2013; Radice et al. 2016; Sekiguchi et al. 2016; Bovard et al. 2017; Dietrich et al. 2017), and (ii) the ejecta velocity  $\gtrsim 0.1\text{--}0.3 c$  required for the blue component is too high for the post-merger ejecta found in numerical-relativity simulations (e.g., Metzger & Fernández 2014; Fujibayashi et al. 2018, which typically show  $\sim 0.05 c$ ).

In these kilonovae/macronovae models (Cowperthwaite et al. 2017; Kasen et al. 2017; Kasliwal et al. 2017; Villar et al. 2017), the contribution from each ejecta component to the lightcurves is separately calculated and composited. However, in reality, the lightcurves are determined through the non-trivial radiation transfer of photons in both ejecta components. In this Letter, we perform an axisymmetric radiative transfer simulation for kilonovae/macronovae taking the interplay of multiple ejecta components of non-spherical morphology into account. We show that the optical and NIR lightcurves of SSS17a can be reproduced by the ejecta model that agrees quantitatively with the prediction of numerical-relativity simulations.

## 2. Method and Model

We derive lightcurves and spectra of kilonovae/macronovae using a wavelength-dependent radiative transfer simulation (Tanaka & Hotokezaka 2013; Tanaka et al. 2017, 2018). The photon transfer is calculated by the Monte Carlo method for given ejecta profiles of density, velocity, and element abundance. The nuclear heating rates are given based on the results of  $r$ -process nucleosynthesis calculations by Wanajo et al. (2014). We also consider the time-dependent thermalization efficiency following an analytic formula derived by Barnes et al. (2016). We update the code so that special-relativistic effects on photon transfer are fully taken into account. The grid resolution of the simulation is also improved by an order of magnitude from our previous works by imposing axisymmetry.

For photon-matter interaction, we consider the same physical processes as in Tanaka & Hotokezaka (2013) and Tanaka et al. (2017, 2018). Bound-bound, bound-free, and free-free transitions and electron scattering are considered for a transfer of optical and NIR photons. For the bound-bound transitions, which have a dominant contribution in the optical and NIR wavelengths, we used the formalism of the expansion opacity (Eastman & Pinto 1993; Kasen et al. 2006). For atomic data, the same line list as in Tanaka et al. (2017) is used. This line list is constructed by the atomic structure calculations for Se ( $Z = 34$ ), Ru ( $Z = 44$ ), Te ( $Z = 52$ ), Nd ( $Z = 60$ ), and Er ( $Z = 68$ ), and supplemented by Kurucz's line list for  $Z < 32$  (Kurucz & Bell 1995). As the atomic data are not complete, we assume the same bound-bound transition properties for the elements with the same open shell as in Tanaka et al. (2018). As the atomic data include only up to doubly ionized ions, our calculations are applicable only for  $\gtrsim 0.5$  days after the merger, during which the temperature is

low enough ( $\lesssim 10,000$  K). The ionization and excitation states are calculated under the assumption of local thermodynamic equilibrium by using the Saha ionization and Boltzmann excitation equations.

Numerical-relativity simulations demonstrate that the post-merger ejecta is surrounded by the dynamical ejecta because the latter has a higher velocity than the former. In such a situation, the post-merger ejecta would irradiate and heat up the dynamical ejecta, helping less-massive dynamical ejecta reproduce long-lasting NIR lightcurves. Furthermore, because the dynamical ejecta has a higher velocity than the post-merger ejecta, the reprocessing of photons in the dynamical ejecta helps to enhance the photospheric velocity. Most of the dynamical ejecta is present near the binary orbital plane (i.e.,  $\theta \gtrsim \pi/4$ ), and only a part of the dynamical ejecta is present in the polar region ( $\theta \leq \pi/4$ ), where  $\theta$  is the inclination angle measured from the orbital axis of the binary (e.g., Hotokezaka et al. 2013; Radice et al. 2016; Sekiguchi et al. 2016). Nevertheless, low-density dynamical ejecta in the polar region can significantly modify the spectrum due to the large opacity determined by lanthanides, known as the lanthanide curtain effect (Kasen et al. 2015; Wollaeger et al. 2017). As the gravitational-wave data analysis of GW170817 infers that the event was observed from  $\theta \gtrsim 28^\circ$  (Abbott et al. 2017a), photon-reprocessing in both the low-density and high-density dynamical ejecta would be important for the lightcurve prediction.

For our radiative transfer simulation, we need the density and velocity profiles of ejecta. Within the range of predictions by numerical-relativity simulations, we set up a model that reproduces the key observational data of SSS17a, such as the lightcurves and photospheric velocity. We employ homologically expanding ejecta composed of two parts; the post-merger ejecta with the velocity from  $v = 0.025 c$  to  $0.08 c$ , and the dynamical ejecta from  $v = 0.08 c$  to  $0.9 c$ , where  $v = r/t$  is the velocity of the fluid elements,  $r$  is the radius, and  $t$  is time measured from the onset of the merger. Note that the presence of the high-velocity components with  $v \gtrsim 0.3 c$  up to  $\sim 0.9 c$  is suggested by the latest high-resolution numerical-relativity simulation (Hotokezaka et al. 2018). We adopt a power-law density distribution of  $\propto r^{-3}$  and  $\propto r^{-6}$  for the post-merger and dynamical ejecta, respectively, following the numerical-relativity results. To take the morphology of the dynamical ejecta into account, the density for  $\theta \leq \pi/4$  is set to be  $\approx 1000$  times smaller than that for  $\theta \geq \pi/4$ , and the low- and high-density regions are smoothly connected employing a logistic function,  $\{1 + \exp[-20(\theta - \pi/4)]\}^{-1}$  (see Figure 1). The total masses of the post-merger and dynamical ejecta are set to be  $0.02 M_{\odot}$  and  $\approx 0.009 M_{\odot}$ , respectively. The latest numerical-relativity simulations show that these are reasonable values (e.g., Hotokezaka et al. 2013; Metzger & Fernández 2014; Dietrich et al. 2017; Fujibayashi et al. 2018). Following the numerical-relativity results (Sekiguchi et al. 2016; Shibata et al. 2017; Fujibayashi et al. 2018), the element abundances are determined by  $r$ -process nucleosynthesis calculations by Wanajo et al. (2014), assuming flat  $Y_e$  distributions from 0.3–0.4 and 0.1–0.4 for the post-merger and dynamical ejecta, respectively.

We note that the density profile and the  $Y_e$  distribution of the dynamical ejecta in the polar region may be lower than the prediction by the numerical-relativity results (see e.g., Radice et al. 2016; Sekiguchi et al. 2016; Bovard et al. 2017).

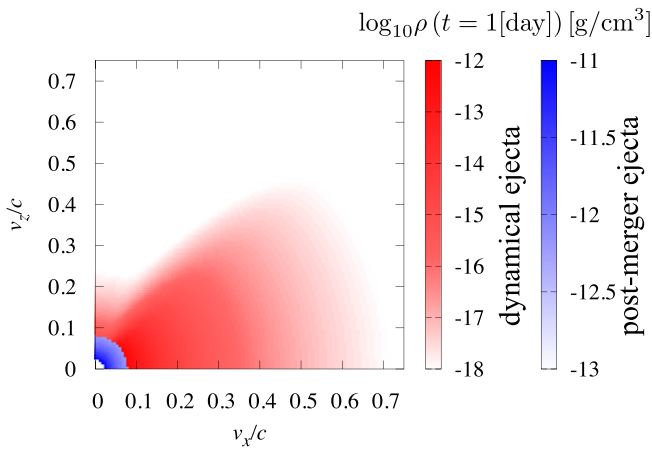


**Figure 1.** Density profile of the ejecta employed in the radiative transfer simulation. The red and blue regions denote the dynamical and post-merger ejecta, respectively. Homologous expansion of the ejecta and axisymmetry with respect to the  $z$ -axis are assumed in the simulation.

However, we find that similar results are obtained by employing  $\approx 40$  times higher density and  $\approx 70$  times less lanthanide fraction in the polar region. Thus, degeneracy is present. By fine-tuning the density and  $Y_e$  distribution, we can find better-fitted models. Because there are many uncertainties in the ejecta model, we construct a model as simple as possible. Employing the solar  $r$ -process abundance instead of  $Y_e = 0.1$ – $0.4$  for the dynamical ejecta makes only a small difference in the results. The post-merger ejecta often has a component of  $Y_e \gtrsim 0.4$ , which does not contribute significantly to heating because the heavy elements are not synthesized from such a component (Wanajo et al. 2014; Kasen et al. 2015). Here, the mass of  $0.02 M_\odot$  required for the post-merger ejecta is for the component with  $Y_e \lesssim 0.4$ . Although it is neglected for simplicity, we note that a small fraction of post-merger ejecta might have a moderately low- $Y_e$  component even if the remnant NS is sufficiently long-lived, and it may be needed to interpret the observed spectra, as we discuss below (Metzger & Fernández 2014; Perego et al. 2014; Lippuner et al. 2017; Fujibayashi et al. 2018).

### 3. Results

Figure 2 compares the observed  $ugriz$ - and  $JHK$ -band lightcurves of SSS17a (Villar et al. 2017) with those of our kilonova/macronova model. As a fiducial model to interpret the lightcurves of SSS17a, we employ the lightcurves observed from  $20^\circ \leq \theta \leq 28^\circ$ , taking into account the results of the gravitational-wave data analysis of GW170817 (Abbott et al. 2017a). We find that both optical and NIR lightcurves of SSS17a are approximately reproduced by a setup motivated by numerical-relativity simulations. In particular, the  $ugri$ - and  $zJHK$ -band lightcurves of the model agree with the data points within 1 mag for  $t \leq 2.5$  days and  $t \leq 9$  days, respectively.

In our model, the long-lasting NIR lightcurves are reproduced by the dynamical ejecta with a mass that is much smaller than that estimated by the previous studies employing a simple composite model of ejecta components (e.g., Cowperthwaite et al. 2017; Kasen et al. 2017; Kasliwal et al. 2017; Villar et al. 2017). This can be understood by considering the irradiation from the post-merger ejecta to the dynamical ejecta. The mass of the post-merger ejecta is also smaller than that estimated by

previous studies. This is due to the preferential diffusion of photons to the polar direction, by which the luminosity is effectively enhanced in the polar direction in the presence of the optically thick dynamical ejecta in the equatorial plane. Indeed, we find that the total luminosity integrated over all of the viewing angles is smaller by a factor of 2–3 than the isotropic luminosity observed from  $20^\circ \leq \theta \leq 28^\circ$  (see also Kasen et al. 2015).

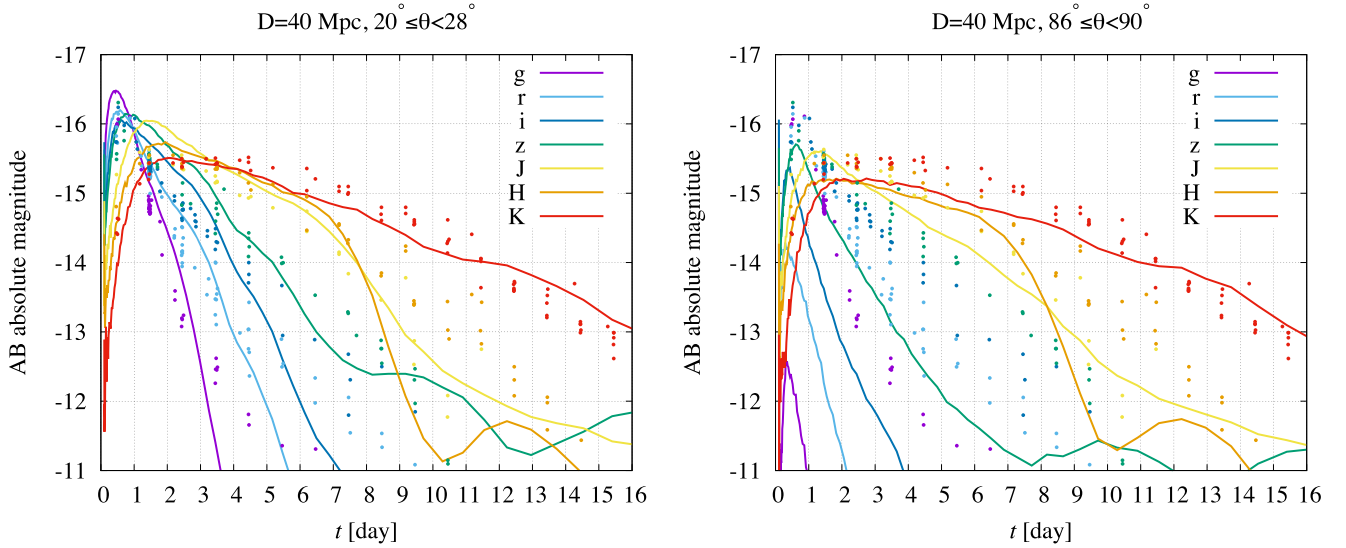
The right panel of Figure 2 shows the lightcurves of the model observed from the equatorial direction ( $86^\circ \leq \theta \leq 90^\circ$ ). The  $ugriz$ -band luminosity is much smaller than that observed from  $20^\circ \leq \theta \leq 28^\circ$ , while similar magnitudes of luminosity are found in the  $JHK$ -bands. This reflects the fact that photons from the post-merger ejecta are entirely absorbed by the dynamical ejecta concentrated in the equatorial plane. This suggests that bright emission in the  $ugriz$ -band as found in SSS17a would not be observed for a similar NS merger if it is observed from the direction of the orbital plane.

Figure 3 shows the time evolution of optical and NIR spectral energy distribution of the kilonova/macronova model observed from  $20^\circ \leq \theta \leq 28^\circ$ . As shown in the multi-color lightcurves, our model reproduces an overall spectral evolution from blue to red with time. The spectra of our model agree approximately with blackbody spectra for  $t \approx 1$ – $7$  days, as is seen in the observation of SSS17a (e.g., Waxman et al. 2018).

Figure 4 shows the (isotropic) bolometric luminosity,  $L_{\text{bol}}$ , effective temperature,  $T_{\text{eff}}$ , photospheric radius,  $r_{\text{ph}}$ , and photospheric velocity,  $v_{\text{ph}}$ , of the kilonova/macronova model.  $T_{\text{eff}}$  and  $r_{\text{ph}}$  are first obtained by the blackbody fit of the spectra, and then,  $L_{\text{bol}}$  and  $v_{\text{ph}}$  are calculated by  $L_{\text{bol}} = 4\pi r_{\text{ph}}^2 \sigma T_{\text{eff}}^4$  and  $v_{\text{ph}} = r_{\text{ph}}/t$ , respectively, where  $\sigma$  is the Stefan–Boltzmann constant. We find that all of these quantities calculated from the lightcurves observed from  $20^\circ \leq \theta \leq 28^\circ$  agree with the observation (Waxman et al. 2018). In particular,  $v_{\text{ph}} \approx 0.3 c$  is realized for  $t \leq 2$  days due to photons reprocessed in the dynamical ejecta. Here we stress that the presence of the low-density dynamical ejecta (or more massive but higher  $Y_e$ ) in the polar region is the key to interpreting the observed value of  $v_{\text{ph}}$ . Indeed, we find that the value of  $v_{\text{ph}}$  cannot be as large as  $0.25 c$  for  $\gtrsim 1$  day if the low-density dynamical ejecta region in  $\theta \leq \pi/4$  is absent.

More detailed spectral features are also of interest for comparison. Chornock et al. (2017), Kasliwal et al. (2017), Nicholl et al. (2017), and Tanvir et al. (2017) have all pointed out that SSS17a shows featureless spectra in optical wavelengths and some line-like features in infrared wavelengths. Similar behavior is indeed found in our model at  $>2$  days. At early times ( $<2$  days), our model shows a narrow features at  $\approx 5000 \text{ \AA}$ , which is not found in the observations. However, given the incompleteness of the line list and simplification in the  $Y_e$  distribution, these features should be more smeared out in reality. Thus, it is too early to extract the velocities from the observed/model spectra, and further improvement and investigation of the model is needed in order to interpret the observed line features more quantitatively.

Figure 4 also shows the photospheric quantities calculated from the lightcurves observed from the equatorial direction ( $86^\circ \leq \theta \leq 90^\circ$ ). The luminosity and temperature of the lightcurves are lower than those observed from  $20^\circ \leq \theta \leq 28^\circ$  by a factor of 3–4 and 2–3 at  $\sim 1$  day, respectively, and a larger radius and higher velocity are realized for the photosphere. These differences clearly reflect the density and



**Figure 2.** Optical and NIR lightcurves of SSS17a compared with the kilonova/macronova model observed from  $20^\circ \leq \theta \leq 28^\circ$  (left panel) and  $86^\circ \leq \theta \leq 90^\circ$  (right panel). The optical and NIR data points are taken from Villar et al. (2017). We assume that SSSa17 is at a distance of 40 Mpc. All of the magnitudes are given in AB magnitudes. Note that the large deviation of the model lightcurves in the  $H$ -band may be due to the incompleteness of the line list for the opacity estimation.

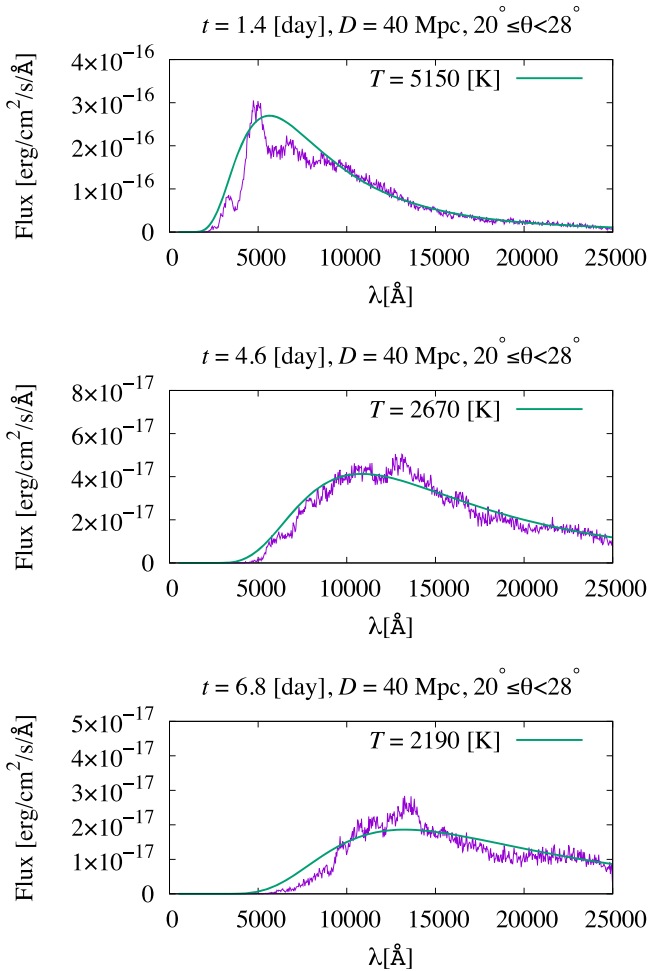


**Figure 3.** Time evolution of optical and NIR spectral energy distribution of the kilonova/macronova model. The spectra at  $t = 1.4, 4.6,$  and  $6.8$  days are shown. All of the spectra are observed from  $20^\circ \leq \theta \leq 28^\circ$  at a distance of 40 Mpc. The green solid curves denote the best blackbody fits of the spectra.

velocity profiles of ejecta such that optically thick dynamical ejecta in the equatorial plane is present outside of the post-merger ejecta.

NS mergers are also considered to be important synthesis sites of  $r$ -process nuclei in the universe (Lattimer & Schramm 1974; Eichler et al. 1989; Korobkin et al. 2012; Wanajo et al. 2014). Figure 5 compares the elemental abundance in our model with the solar abundance. Though some abundance peaks are smaller than those of the solar abundance, broadly speaking, the mass-averaged element abundance of our model reproduces the trend of the solar abundance for a wide range of  $r$ -process elements, in particular, including the first ( $Z = 34$ ) abundance peaks.

#### 4. Discussion and Conclusion

In this Letter, we have presented the result of an axisymmetric radiative transfer simulation for a kilonova/macronova with a setup indicated by numerical-relativity simulations. In particular, the interplay of multiple non-spherical ejecta components via photon transfer are consistently taken into account in the lightcurve prediction.

We found that the optical and NIR lightcurves of SSS17a are reproduced naturally by the numerical-relativity-simulation-motivated model observed from  $20^\circ \leq \theta \leq 28^\circ$ . In particular, we demonstrated that the observed NIR lightcurves can be interpreted by the emission from the dynamical ejecta of which mass is consistent with the prediction of numerical relativity. The observed lightcurves are reproduced by a smaller mass of the post-merger ejecta than that estimated by previous studies (e.g., Cowperthwaite et al. 2017; Kasen et al. 2017; Kasliwal et al. 2017; Perego et al. 2017; Villar et al. 2017) because the effect of the photon diffusion preferential to the polar direction is taken into account. The observed blue optical lightcurves, as well as the photospheric velocity of  $\approx 0.3c$ , can be interpreted by the photon-reprocessing in the low-density dynamical ejecta located in the polar region above the post-merger ejecta.

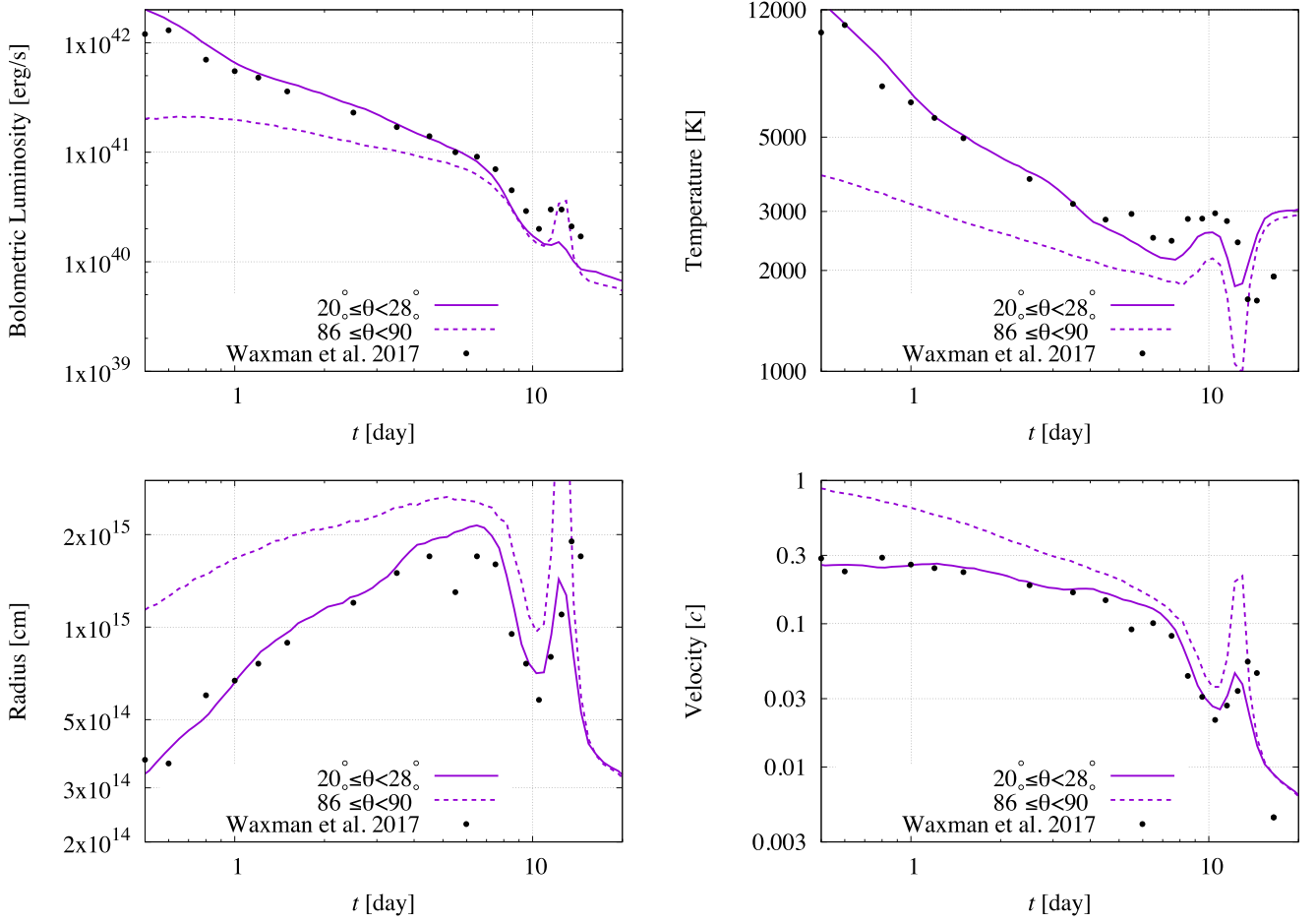


**Figure 4.** Bolometric luminosity ( $L_{\text{bol}}$ ; top-left panel), effective temperature ( $T_{\text{eff}}$ ; top-right panel), photospheric radius ( $r_{\text{ph}}$ ; bottom-left panel), and photospheric velocity ( $v_{\text{ph}}$ ; bottom-right panel) of the kilonova/macronova model of SSS17a.  $L_{\text{bol}}$  and  $v_{\text{ph}}$  are calculated by  $L_{\text{bol}} = 4\pi r_{\text{ph}}^2 \sigma T_{\text{eff}}^4$  and  $v_{\text{ph}} = r_{\text{ph}}/t$ , respectively, using  $T_{\text{eff}}$  and  $r_{\text{ph}}$  obtained by the blackbody fit of the spectra. The solid and dashed curves denote the quantities calculated from the lightcurves observed from  $20^\circ \leq \theta \leq 28^\circ$  and  $86^\circ \leq \theta \leq 90^\circ$ , respectively. The black points denote the data points of SSS17a taken from Waxman et al. (2018).

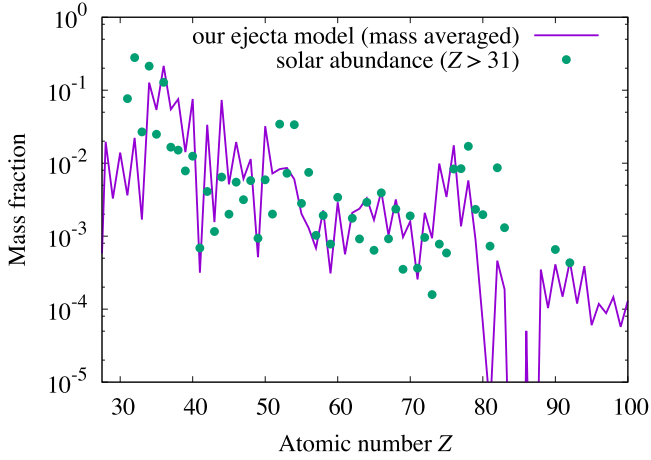


**Figure 5.** Mass-averaged element abundance of our model (blue lines) together with the solar abundance of  $r$ -process elements (Simmerer et al. 2004, green points).

Our results indicate that there is no tension between the prediction of numerical-relativity simulations and the observation of SSS17a, and that the interplay of the multiple non-spherical ejecta components plays a key role for predicting kilonova/macronova lightcurves. Note that Perego et al. (2017), Tanvir et al. (2017), and Troja et al. (2017) showed kilonova/macronova models employing a similar setup with

our model, but did not discuss the high photospheric velocities. In particular, Tanvir et al. (2017) and Troja et al. (2017) used the model based on radiative transfer simulations in which photon interplay between the two components is taken into account (Wollaeger et al. 2017). In these works, the mass of dynamical ejecta is estimated to be an order of magnitude smaller than our result due to the difference in the treatment of line opacity. Note that our model requires  $\sim 0.01 M_{\odot}$  as the mass of the dynamical ejecta. This is a fairly large value for the dynamical ejecta, which can be achieved only for the case that the NS radii are small (e.g., Hotokezaka et al. 2013; Dietrich et al. 2017). Thus, our analysis suggests that the NS radius would be small as  $\lesssim 12$  km.

We found that photons from the post-merger ejecta would be absorbed and entirely reprocessed by the dynamical ejecta, in particular if the binary is observed from the equatorial direction. However, this viewing angle dependence would be minor for the case that the total mass of the binary is smaller than GW170817. For such a case, the mass of the dynamical ejecta would be much smaller ( $\sim 10^{-3} M_{\odot}$  or less; Foucart et al. 2016), and thus suppression of the blue optical emission would be weaker. Furthermore, a long-lived remnant NS is likely to be formed after the merger, and the lightcurves could be significantly modified by the heating up of the ejecta due to the EM radiation from the strongly magnetized and rapidly rotating remnant NS (e.g., Metzger & Piro 2014).

While our kilonova/macronova model of SSS17a agrees approximately with the observation, some deviation from the data points, for example  $\gtrsim 2$  mag differences in the *ugri*- and *zJHK*-bands for  $t \geq 3$  days and  $t \geq 11$  days, respectively, is also found. This may be due to the simplification of the  $Y_e$  distribution in our model, in which we neglect its local dependence found in the simulations (e.g., Metzger & Fernández 2014; Sekiguchi et al. 2016; Bovard et al. 2017; Fujibayashi et al. 2018). We suspect that the deviation of the mass-averaged abundance pattern from the observation found in Figure 5 might be due to the same reason. The incompleteness of the line list for the opacity estimation is also an issue. For example, we suspect that the large deviation found in the model lightcurves in the *H*-band may be due to the simplification that the same bound-bound transition properties are used for the elements with the same open shell. Thus, employing a detailed ejecta profile based on numerical-relativity simulations and more realistic opacity tables are needed in order to reproduce the observation, including the spectra, more accurately.

We thank S. Fujibayashi, K. Hotokezaka, and E. Waxman for valuable discussions. Numerical computation was performed on Cray XC30 at Center for Computational Astrophysics of National Astronomical Observatory of Japan and on Hydra at Max Planck Computing and Data Facility. This work was supported by Grant-in-Aid for Scientific Research (JP16H02183, JP16H06342, JP17H01131, JP15K05077, JP17K05447, JP17H06361, JP15H02075, JP17H06363) of JSPS and by a post-K computer project (Priority issue No. 9) of Japanese MEXT. K.K. was supported by JSPS overseas research fellowships.

### ORCID iDs

Masaru Shibata  <https://orcid.org/0000-0002-4979-5671>  
Masaomi Tanaka  <https://orcid.org/0000-0001-8253-6850>

### References

- Abbott, B., Abbott, R., Abbott, T. D., et al. 2017a, *PhRvL*, **119**, 161101  
 Abbott, B. P., Abbott, R., Abbott, T. D., et al. 2017b, *ApJL*, **848**, L13  
 Barnes, J., Kasen, D., Wu, M.-R., & Martínez-Pinedo, G. 2016, *ApJ*, **829**, 110  
 Bauswein, A., Goriely, S., & Janka, H. T. 2013, *ApJ*, **773**, 78  
 Bovard, L., Martin, D., Guercilena, F., et al. 2017, *PhRvD*, **96**, 124005  
 Chornock, R., Berger, E., Kasen, D., et al. 2017, *ApJL*, **848**, L19  
 Coulter, D. A., Foley, R. J., Kilpatrick, C. D., et al. 2017, *Sci*, **358**, 1556  
 Cowperthwaite, P. S., Berger, E., Villar, V. A., et al. 2017, *ApJL*, **848**, L17  
 Dessart, L., Ott, C., Burrows, A., Rosswog, S., & Livne, E. 2009, *ApJ*, **690**, 1681  
 Dietrich, T., Ujevic, M., Tichy, W., Bernuzzi, S., & Bruegmann, B. 2017, *PhRvD*, **95**, 024029  
 Drout, M. R., Piro, A. L., Shappee, B. J., et al. 2017, *Sci*, **358**, 1570  
 Eastman, R. G., & Pinto, P. A. 1993, *ApJ*, **412**, 731  
 Eichler, D., Livio, M., Piran, T., & Schramm, D. N. 1989, *Natur*, **340**, 126  
 Foucart, F., Haas, R., Duez, M. D., et al. 2016, *PhRvD*, **93**, 044019  
 Fujibayashi, S., Kiuchi, K., Nishimura, N., Sekiguchi, Y., & Shibata, M. 2018, *ApJ*, **860**, 64  
 Hotokezaka, K., Kiuchi, K., Kyutoku, K., et al. 2013, *PhRvD*, **87**, 024001  
 Hotokezaka, K., Kiuchi, K., Shibata, M., Nakar, E., & Piran, T. 2018, arXiv:1803.00599  
 Just, O., Bauswein, A., Pulpillo, R. A., Goriely, S., & Janka, H. T. 2015, *MNRAS*, **448**, 541  
 Kasen, D., Badnell, N. R., & Barnes, J. 2013, *ApJ*, **774**, 25  
 Kasen, D., Fernández, R., & Metzger, B. 2015, *MNRAS*, **450**, 1777  
 Kasen, D., Metzger, B., Barnes, J., Quataert, E., & Ramirez-Ruiz, E. 2017, *Natur*, **551**, 80  
 Kasen, D., Thomas, R. C., & Nugent, P. 2006, *ApJ*, **651**, 366  
 Kasliwal, M. M., Nakar, E., Singer, L. P., et al. 2017, *Sci*, **358**, 1559  
 Korobkin, O., Rosswog, S., Arcones, A., & Winteler, C. 2012, *MNRAS*, **426**, 1940  
 Kulkarni, S. R. 2005, arXiv:astro-ph/0510256  
 Kurucz, R. L., & Bell, B. 1995, Atomic Line List (Cambridge, MA: Smithsonian Astrophysical Observatory)  
 Lattimer, J. M., & Schramm, D. N. 1974, *ApJL*, **192**, L145  
 Li, L.-X., & Paczynski, B. 1998, *ApJL*, **507**, L59  
 Lippuner, J., Fernández, R., Roberts, L. F., et al. 2017, *MNRAS*, **472**, 904  
 Metzger, B. D., & Fernández, R. 2014, *MNRAS*, **441**, 3444  
 Metzger, B. D., Martínez-Pinedo, G., Darbha, S., et al. 2010, *MNRAS*, **406**, 2650  
 Metzger, B. D., & Piro, A. L. 2014, *MNRAS*, **439**, 3916  
 Mooley, K. P., Nakar, E., Hotokezaka, K., et al. 2018, *Natur*, **554**, 207  
 Nicholl, M., Berger, E., Kasen, D., et al. 2017, *ApJL*, **848**, L18  
 Perego, A., Radice, D., & Bernuzzi, S. 2017, *ApJL*, **850**, L37  
 Perego, A., Rosswog, S., Cabezón, R. M., et al. 2014, *MNRAS*, **443**, 3134  
 Radice, D., Galeazzi, F., Lippuner, J., et al. 2016, *MNRAS*, **460**, 3255  
 Rosswog, S., Liebendoerfer, M., Thielemann, F. K., et al. 1999, *A&A*, **341**, 499  
 Sekiguchi, Y., Kiuchi, K., Kyutoku, K., Shibata, M., & Taniguchi, K. 2016, *PhRvD*, **93**, 124046  
 Shibata, M., Fujibayashi, S., Hotokezaka, K., et al. 2017, *PhRvD*, **96**, 123012  
 Siegel, D. M., & Metzger, B. D. 2017, *PhRvL*, **119**, 231102  
 Simmerer, J., Sneden, C., Cowan, J. J., et al. 2004, *ApJ*, **617**, 1091  
 Smartt, S. J., Chen, T.-W., Jerkstrand, A., et al. 2017, *Natur*, **551**, 75  
 Tanaka, M., & Hotokezaka, K. 2013, *ApJ*, **775**, 113  
 Tanaka, M., Kato, D., Gaigalas, G., et al. 2018, *ApJ*, **852**, 109  
 Tanaka, M., Utsumi, Y., Mazzali, P. A., et al. 2017, *PASJ*, **69**, 102  
 Tanvir, N. R., Leván, A. J., González-Fernández, C., et al. 2017, *ApJL*, **848**, L27  
 Troja, E., Piro, L., van Eerten, H., et al. 2017, *Natur*, **551**, 71  
 Valenti, S., Sand, D. J., Yang, S., et al. 2017, *ApJL*, **848**, L24  
 Villar, V. A., Guillochon, J., Berger, E., et al. 2017, *ApJL*, **851**, L21  
 Wanajo, S., Sekiguchi, Y., Nishimura, N., et al. 2014, *ApJ*, **789**, 39  
 Waxman, E., Ofek, E. O., Kushnir, D., & Gal-Yam, A. 2018, *MNRAS*, <https://academic.oup.com/mnras/advance-article/doi/10.1093/mnras/sty2441/5091828>  
 Wollaeger, R. T., Korobkin, O., Fontes, C. J., et al. 2018, *MNRAS*, **78**, 3298